Proceedings of the 16th International Conference on Soil Mechanics and Geotechnical Engineering

doi:10.3233/978-1-61499-656-9-2559

Real-time prediction of rainfall-induced instability in sandy slopes

Prévision en temps réel de l'instabilité induite par précipitations des pentes sableuses

R.P. Orense
Chuo Kaihatsu Corporation, Tokyo, Japan
S. Shimoma
Shimizu Corporation, Iwate, Japan
K. Farooq
University of Engineering and Technology, Lahore, Pakistan

ABSTRACT
Landslides occur frequently during or following periods of heavy rainfall. In order to understand the mechanism and conditions leading to these slope failures, a comprehensive testing program consisting of constant shear stress drained triaxial tests and model slope experiments was performed using sandy material obtained from a former landslide site. Results of both element tests and model experiments clearly showed that slope failure is induced due to the development of pore-water pressure in slope. As soil moisture contents within the slope approach critical values, ground deformations are mobilized. Therefore, by properly selecting regions where the soil moisture contents must be monitored, possibly in areas where seepage forces will develop, failure initiation in slopes can be predicted. Based on this, a simple monitoring scheme to predict in real-time the occurrence of failures in critical slopes was proposed.

RÉSUMÉ
Les glissements de terrain se produisent fréquemment pendant ou après des périodes de fortes précipitations. Afin de comprendre le mécanisme et les conditions menant à de telles ruptures de pentes, une étude complète composée de tests triaxiaux drainés avec effort de cisaillement constant ainsi que d'expériences sur des modèles de pentes a été realisée avec des matériaux sableux récupérés sur le site d'un ancien glissement de terrain. Les résultats de l'ensemble de ces tests, à la fois triaxiaux et sur les modèles, montrent que les ruptures de pente prennent place suite au développement de pressions dans les pores remplis d'eau de la pente. Alors que le degré d'humidité du sol approche des valeurs critiques, des déformations dans le sol sont observées. Par conséquent, en sélectionnant correctement les zones dans lesquelles les mesures d'humidité du sol doivent être effectuées, c'est à dire celles où les forces d'infiltration risquent de se développer, il est possible de prévoir l'apparition d'une rupture dans la pente. Basé sur ceci, un système simple de mesures pour prévoir en temps réel l'apparition de ruptures dans les pentes critiques a été proposé

1 INTRODUCTION

Failures in slopes that are marginally stable and formed by loosely compacted residual and colluvial soils occur frequently during or following periods of heavy rainfall. While the cause of these failures has been attributed mainly to the reduction in available shear strength of soil as a result of loss in suction and increase in positive pore-water pressure, current understanding of the mechanism and conditions on how slope deformation can be initiated is still insufficient to develop appropriate and efficient warning system to minimize the associated risk.

To address this issue, a comprehensive testing program was carried out in the laboratory to investigate factors affecting initiation of rainfall-induced landslides. Constant shear stress drained triaxial tests on initially unsaturated specimens were conducted to simulate the stress path followed by soil element in a slope during rainfall (Figure 1). In these tests, total normal stress, σ_n, and shear stress, τ, essentially remained constant during the process of rainwater infiltration (Brand, 1981: Brenner et al., 1985). In addition to pore-water pressure inside the specimen, axial and volumetric strains during water infiltration were examined. To supplement the results, seepage and rainfall tests on instrumented small-scale model slopes were also performed. Pore-water pressure, slope deformation and soil moisture contents at specified points within the slope were monitored. Based on the results of these tests, a simple methodology was proposed to predict in real-time the occurrence of failures in critical slopes and to determine if the failed portion of slope mass would impact important facilities located near the bottom of the slope.

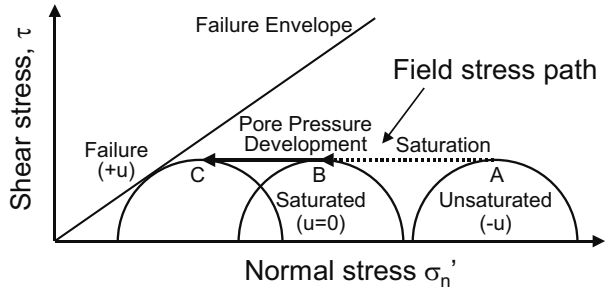

Figure 1. Field stress path in a slope subjected to rainwater infiltration

2 EXPERIMENTAL SET-UP

2.1 *Materials used*

The materials employed in both laboratory triaxial and model tests were obtained from Omigawa, Chiba Prefecture (Japan), site of more than 250 landslides associated with the passage of Typhoon No. 25 in September 1971 (Chiba Prefecture, 1972). The materials were generally sandy in nature, and the physical properties are summarized in Table 1.

2.2 *Constant shear stress drained tests*

In element tests, an automated stress-controlled triaxial test apparatus was employed. It is equipped with a high air-entry value (300 kPa) ceramic disk at the bottom to measure initial suction of the unsaturated specimen. The soil specimen, 155 mm high and 75 mm in diameter, was prepared on top of the saturated ceramic disk by wet tamping method at specified initial relative density, *Dr*, and initial moisture content, *w*. A 12 mm-long

Table 1: Properties of Omigawa sand

Specific gravity, *Gs*	2.67
Mean grain size, D_{50} (mm)	0.49
Gravel content (%)	0.5
Sand content (%)	90.1
Fines content (%)	9.4
Coefficient of uniformity, C_u	6.17
Coefficient of gradation, C_c	1.70
Maximum void ratio, e_{max}	1.07
Minimum void ratio, e_{min}	0.71
Plasticity index, *Ip*	NP

pore-water pressure transducer was placed at one-third height of the specimen to monitor changes in pore-water pressure, *u*. The specimen was first isotropically consolidated and then axial stress was increased to a specified level of principal stress ratio ($K=\sigma_1/\sigma_3$) to represent field consolidation state of in-situ soil along a potential failure plane. Because typical depths of failure in actual slopes are quite shallow, testing was conducted at low effective confining pressure (σ_3=15~50 kPa). After full consolidation, water was slowly infiltrated through the bottom ceramic disk until the specimen failed.

During water infiltration, deformation of the specimen was continuously monitored using clip gages and linear variable displacement transducer (LVDT), while axial stress was kept constant by a computer. In line with the assumption that pore-air pressure in shallow slopes remained atmospheric, the top cap was vented to the atmosphere. Furthermore, volume of water entering and leaving the sample was also carefully measured.

2.3 *Small- scale model experiments*

To supplement the triaxial test results and to observe general failure pattern of slopes during rainfall, a series of model slope tests was performed. The soil box employed is 220 cm long, 80 cm wide and 100 cm high (see Figure 2). Its walls are made of steel plates, except for the front side which is made of transparent acryl glass for observing the deformation process. The model slopes were constructed in the center portion of the box by laying out Omigawa sand (initial *w*=10%) in series of horizontal layers, where each layer was tamped equally to achieve a prescribed density. Pore-water pressure meters, soil moisture content transducers (Amplitude Domain Reflectometry or ADR-type) and a shear displacement transducer were installed within the model slope. In addition, pin markers were set on the slope surface as well as on the side adjacent to the acryl glass wall to examine ground displacements using two video cameras set-up at strategic locations.

In the tests, failure was initiated in the small-scale model slope either through seepage from water supply chamber located upslope (as shown in Figure 2 to simulate percolating water from upslope in natural ground during rainfall) or through seepage by artificial rainfall using hoses and nozzles. Because of scale effects, it is worthy to mention that the tests were conducted to investigate the general behavior of slopes and were not meant to simulate in-situ conditions.

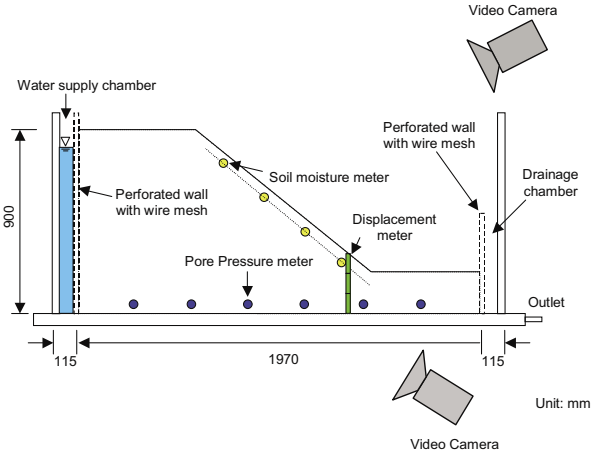

Figure 2. Schematic diagram of the soil box and the sensor locations

3 EXPERIMENTAL RESULTS AND DISCUSSIONS

3.1 *Element tests*

In the experimental program, effects of various parameters related to the initial condition of the specimen were investigated. These parameters include initial relative density, *Dr*; initial principal stress ratio, *K*; initial degree of saturation, *Sr*; initial confining pressure, σ_3; and infiltration rate, *Q*. Due to space limitation, only limited test results are discussed here. Other test results are presented elsewhere (Farooq et al., 2004).

Figure 3 shows the results of constant shear stress drained tests on initially unsaturated samples (initial *Sr*=20%) in which initial conditions of *K*=2.5 and σ_3=25 kPa were kept constant, while *Dr* was varied from 41~79%. Values of over-all *Sr* shown in the figure refer to the average within the whole specimen. Notice from Figure 3(a) that there was continuous but gradual development of axial strain, ε_a, during the initial phase of water infiltration. After a certain time had elapsed, the specimen reached its yield point and axial strain increased suddenly. This point is defined as the failure initiation of the soil specimen. Once failure initiation point was reached (denoted by ⊗ in the figure), the development of ε_a progressed rapidly and large strains (>10%) were reached in relatively short time. Values of *Sr* when failure was induced were in the range of 90~91% for all specimens.

Strain rates before ($\dot{\varepsilon}_1$) and after ($\dot{\varepsilon}_2$) failure initiation were measured in all specimens, and it was observed that both strain rates increased as *Dr* decreased. This observation implies that loose soil slopes would undergo more rapid deformation than dense ones when subjected to rainfall infiltration.

Figure 3(b) shows the variation of monitored pore-water pressure inside the sample. Note that although there was negative pore-water pressure (soil suction) present within the specimen during the initial phase of water infiltration, it was not read by the miniature transducer as it could measure only positive values. In all tests, there was an increase in pressure of about 2~3 kPa, followed by gradual decrease. Such increase may have been caused by pore-air pressure as the infiltrating water pushed up the entrapped air from the bottom portion of the specimen. Since the top end of the specimen was vented to the atmosphere, the pressure dissipated gradually.

When sufficient level of *Sr* was attained within the specimen, pore-water pressure started to increase and, consequently, fail-

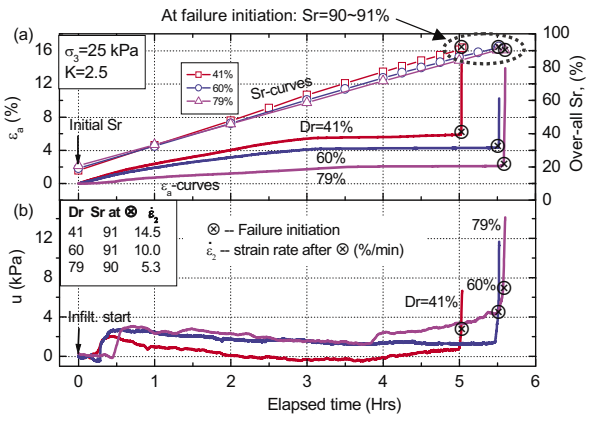

Figure 3. Time histories of: (a) axial strain, ε_a, and over-all degree of saturation, *Sr*; (b) pore water pressure, *u*, showing the effect of varying relative density, *Dr*

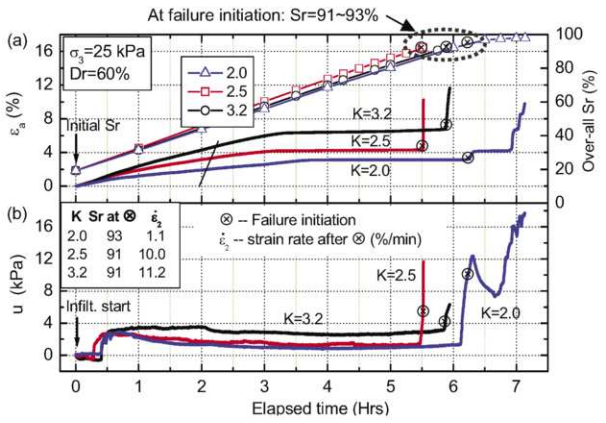

Figure 4. Time histories of: (a) axial strain, ε_a, and over-all degree of saturation, *Sr*; (b) pore water pressure, *u*, showing the effect of principal stress ratio, *K*

ure was initiated within the specimen. It can be surmised from Figure 3 that the sudden increase in pore-water pressure is preceded by the reduction in initial suction within the specimen following the saturation process.

Results considering the effects of initial principal stress ratio *K*, indicative of degree of slope inclination, are shown in Figure 4. In these tests, initial *Dr*=60% and σ_3=25 kPa were kept constant and values of initial *K* were varied from 2.0~3.2. As in previous case, test results showed practically bi-linear deformation time history, i.e., very small axial strains during the initial phase of water infiltration followed by rapid increase once failure initiation point was reached. Moreover, failure was induced in soil specimens at essentially constant *Sr* (=91~93%), irrespective of initial *K*.

Detailed examination of Figure 4(a) shows that strain rates before ($\dot{\varepsilon}_1$) and after ($\dot{\varepsilon}_2$) failure initiation are greater for higher values of *K*, indicating that more rapid ground movement would be expected for steeper slopes than for mild ones. This observation is consistent with the general idea that slope gradient is a significant factor in establishing the instability state as well as the post-failure initiation condition of slopes.

3.2 *Model tests*

In model tests, effects of initial relative density, *Dr*, slope inclination, θ, slope model shape and rainfall intensity, *R*, were examined. Again, due to space limitation, only two cases are presented herein. Other test results are discussed in detail by Orense et al. (2004).

The model slope used in Case 1 was 70 cm high, with inclination θ=40° and *Dr*=50%. Slope instability was induced by supplying water to the upslope end by maintaining 80 cm height of water in the supply chamber (see Figure 2). With the difference in pressure head between the supply chamber and the rest of the slope, water percolated into the ground. Figure 5 shows the monitored time histories of displacement (near the toe of slope), volumetric water contents (θ_s) and pore-water pressures (PWP) at the sensor locations. The progress of wetting front within the slope is indicated by the temporal development of pore-water pressure. The pore pressure readings show gradual increase in pore-water pressure, starting from the left side of the slope, consistent with the movement of the wetting front. When the region where M1 and M2 sensors were located was saturated (corresponding to *Sr*=90%), the ground started to deform in a very rapid manner. The maximum surface displacement near the toe was about 8 cm, while deformation 5 cm below the surface was 4 cm. This indicates that only superficial portion of the slope was involved in the movement.

Case 2 corresponds to a similar slope but with an impermeable base located 30 cm from the slope surface. For this case, instability was induced through seepage by artificial rainfall generated using hoses and nozzles set-up adjacent to the experimental box. Rainfall gauges were placed at two locations, one on the top and another at the bottom of the slope, and the accumulated rainwater was measured periodically. The monitored rainfall intensity was about *R*=42~72 mm/hr.

Figure 6 shows the time histories of toe displacement, moisture contents and pore-water pressures. At about *t*=1000 sec, the infiltrating rainwater reached the soil moisture transducers located 5 cm from the ground surface, and the soil moisture contents increased simultaneously. However, they remained constant as the wetting front progressed downward toward the impermeable base. As infiltration continued, a water table developed at the base of the slope, and pore-water pressure increased at P1 and P2 (at about *t*=5600 sec). As the water table approached M2 location, the soil moisture content at this point increased and when it registered θ_s=0.42 (equivalent to *Sr*=90%), the slope began to move. Displacement of about 14 cm was recorded near the toe of the slope.

In both tests, detailed examination of the movement of the surface pins recorded by video cameras revealed that small-scale movements and tensile crack formation preceded the onset of failure. Cracks were formed due to the decrease in strength at the slip surface related to the pore-water pressure increase. This indicates that occurrence of minute slope deformations can also serve as indicator of impending slope failure.

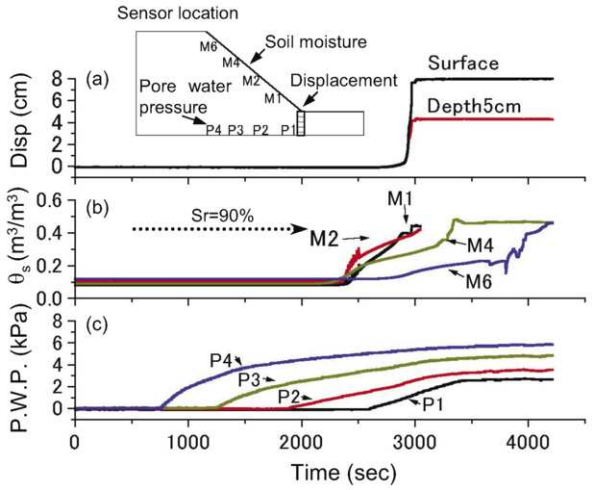

Figure 5. Time histories of: (a) toe displacement; (b) volumetric water content; (c) pore-water pressure at sensor locations (Case 1: seepage test)

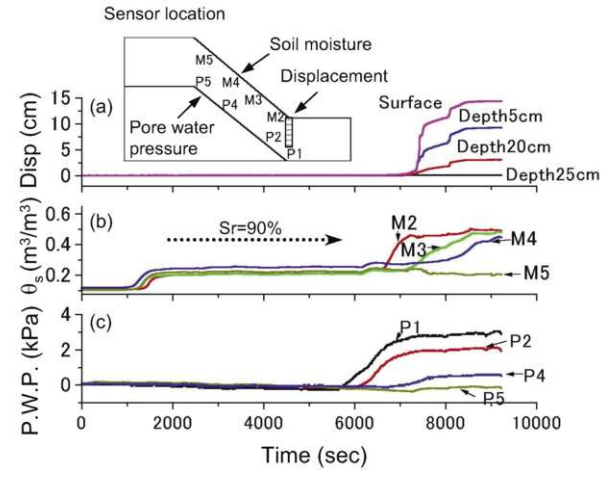

Figure 6. Time histories of: (a) toe displacement; (b) volumetric water content; (c) pore-water pressure at sensor locations (Case 2: rainfall test)

4 PROPOSED MONITORING SCHEME

The above test results clearly demonstrated the possibility of predicting the time to failure initiation by monitoring changes in soil moisture content within the slope. Soil moisture sensors can be installed at critical locations, possibly in areas where seepage forces will develop. This can be supplemented by slope displacement monitoring (by tiltmeter, GPS-based system, etc.).

With these in mind, a simple monitoring scheme to mitigate damage to important facilities due to slope failures is proposed. First, the potential slip plane in the critical slope is assumed. The results of model tests indicate the inclinations of the remaining portion of the slopes after failure (defined as residual slope angle α_{res}) are the same for all cases. For Omigawa soil, it was observed from model tests that α_{res}=20^o (Orense et al., 2004). Thus, as shown in Figure 7(a), failure is assumed to involve the triangular region above α_{res} where soil moisture content exceeds the threshold value corresponding to the soil type present in the slope (e.g., *Sr*=90~91% for Omigawa soil).

Next, the travel distance of the failed portion of the slope is estimated. For this purpose, results of field survey done by Moriwaki (1987) on actual slope failures due to rainfall are used. The results, shown as black dots in Figure 7(b), showed a linear relation between the slope tangent at the source area and the ratio of slope height to travel distance. The results of all model tests are also plotted in the figure and a good agreement is observed. In using these results, the lower limit shown by the dashed line is employed to be on the safe side. Now, the slope tangent at the source area is generally known from the profile. When the travel distance, *L*, necessary to impact an important facility is known, the volume of slope involved in failure, which is a function of *H*, can be estimated. Thus, in the proposed scheme, real-time prediction not only of whether the slope will fail or not, but also the extent of the failed mass and whether it could impact a facility located downslope can be performed.

The proposed scheme is shown schematically in Figure 8. For a given rainfall data shown in Figure 8(a), moisture contents within the slope will rise, possibly starting with that near the toe (Figure 8b). From the moisture readings, the expansion of saturated region above the slip surface can be assessed in real-time and estimates of failed soil volume and the corresponding travel distance can be made (Figure 8c). When the estimated travel distance *L* reaches a critical value (L_{crit}) such that it would impact the facility downslope, a warning is issued. The warning is cancelled when the estimated *L* drops below L_{crit}.

One advantage of this method is that installation of many moisture sensors along the slope is not necessary. Monitoring can be done only at the height corresponding to L_{crit} (e.g., M3 in Figure 8). Moreover, if details of ground conditions (topography, soil properties) are known, monitoring of groundwater table and precipitation, as well as unsaturated seepage analysis and slope stability study, can be employed to supplement the assessment. Thus, a low-cost prediction system can be established. Since the system cannot predict the collapse time with high degree of accuracy, alarm can be issued several tens of minutes prior to reaching L_{crit} to give residents or transport operators sufficient time to respond.

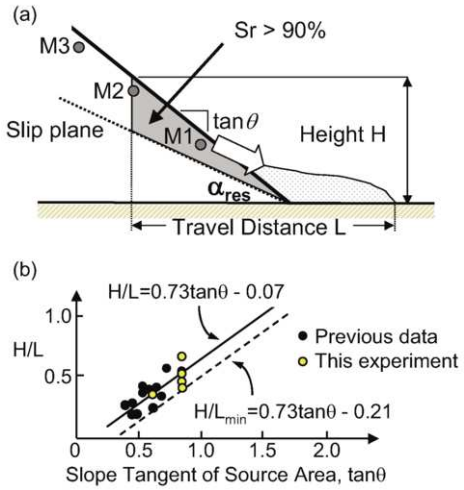

Figure 7. Basis of monitoring scheme: (a) zone with high potential to sliding; (b) relation between *H*/*L* and slope tangent of slide source area

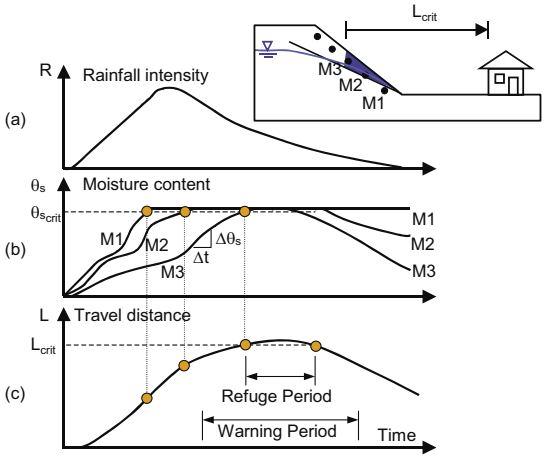

Figure 8. Schematic diagram showing the time histories of: (a) rainfall, *R*; (b) moisture content, θ_s; (c) travel distance, *L*

Slope displacement monitoring is also necessary since retrogressive type of failure may occur. Furthermore, in case warning alarm is issued, it may be necessary to conduct measures such as patrolling the affected area, rescue activities and restoration works. During this period, displacement monitoring can be employed to minimize secondary damage.

5 CONCLUDING REMARKS

Constant shear stress drained triaxial tests and seepage/rainfall tests on small-scale model slopes were performed to investigate failure initiation in sandy slopes due to rainwater infiltration. Test results showed that failure was induced due to the development of pore-water pressure within the slope. As the soil moisture contents approached saturated values, ground deformations were mobilized. Moreover, failures were generally preceded by minute slope displacements. From these results, a simple methodology was proposed to predict in real-time the occurrence of rainfall-induced slope failures by carefully monitoring changes in soil moisture contents and deformations at critical locations within the slope. Then, appropriate warning can be issued to mitigate damage to facilities downslope. Further investigations by numerical analyses and/or actual in-situ monitoring are necessary to validate the proposed system.

REFERENCES

Brand, E.W. (1981). Some thoughts on rain-induced slope failures. *Proc., 10th ICSMFE*, Stockholm, 3, 373-376.

Brenner R.P., Tam, H.K. and Brand, E.W. (1985). Field stress path simulation of rain-induced slope failure. *Proc., 11th ICSMFE*, San Francisco, 2, 991-996.

Farooq, K. Orense, R. and Towhata, I. (2004). Response of unsaturated sandy soils under constant shear stress drained condition. *Soils and Foundations*, 44 (2), 1-13.

Chiba Prefecture, Civil & River Division (1972). *Report of Disaster in Chiba caused by Autumn Rain Front of September 6-7, 1971 and Typhoon No. 25* (in Japanese).

Moriwaki, H. (1987). Prediction of distance attained by failed slopes. *Landslides*, 24 (2), 10-16 (in Japanese).

Orense, R.P., Shimoma, S., Maeda, K. and Towhata, I. (2004). Instrumented slope failure due to water seepage. *Journal of Natural Disaster Science*, 26 (1), 15-26.